Facile Epoxidation Strategy for Producing Amphiphilic Up-Converting Rare-Earth Nanophosphors as Biological Labels

He Hu, Mengxiao Yu, Fuyou Li,* Zhigang Chen, Xia Gao, Liqin Xiong, and Chunhui Huang

Department of Chemistry & Laboratory of Advanced Materials, Fudan University, 220 Handan Road, Shanghai 200433, China

Received May 4, 2008. Revised Manuscript Received September 15, 2008

The biological application of up-converting rare-earth nanophosphors (UCNPs) is still restricted because of unfavorable surface properties. Herein, the development of a simple, effective, and versatile method for converting hydrophobic UCNPs into amphiphilic ones, based on epoxidation of the surface oleic acid (OA) ligand and further coupling with polyethylene glycol monomethyl ether (mPEG-OH), is described. The successful epoxidation and effective coating of the surface of the UCNPs by mPEG-OH have been confirmed by ^{1}H NMR spectrometry, Fourier-transform infrared (FTIR) spectroscopy, and dynamic light scattering (DLS) studies. Investigations by transmission electron microscopy (TEM) and photoluminescence (PL) spectroscopy showed no obvious variations in the morphologies and luminescent properties of the UCNPs during the epoxidation and functionalization processes. In particular, the low cytotoxicity and good cell membrane permeability of the resulting amphiphilic mPEG-UCNPs make them promising candidates for use as bioimaging probes.

1. Introduction

Nanosized luminescent materials have great potential applications in biological studies. This has come to the fore since the pioneering work on quantum dots (QDs) as biological labels by the groups of Alivisatos and Nie.[1] In particular, QDs with tunable size-dependent emissions, high fluorescence quantum yields, and broad excitation spectra have been widely developed and applied in biological analyses.[1a,b] However, owing to the use of short-wavelength (high-energy) photon excitation,[2] these down-conversion luminescent nanomaterials still suffer from some drawbacks, including low light-penetration depth, possible severe photodamage to living organisms, and strong background fluorescence (noise) of some biological samples.[3] The subsequent implementation in this context of two-photon technology[3a,b] greatly reduced these problems by using excitation with long-wavelength femtosecond pulses ($\sim 1 \times 10^{-13}$ s) at a high repetition rate (typically ~80 MHz). Unfortunately, however, because of its low efficiency, two-photon excitation requires enormously high light intensities, which if continuous, would almost instantly vaporize the specimen.[3c]

Alternatively, up-conversion luminescence (UCL)[4] can be used, taking advantage of its unique process in which low-energy light, usually NIR, is converted into higher-energy light (visible) through sequential absorption and energy-transfer steps.[5] Lanthanide ions are suitable candidates for up-conversion processes because of their unique 4f electronic structure and energy levels.[5a] Under continuous-wave (CW) excitation at 980 nm, lanthanide-doped rare-earth phosphors exhibit unique up-conversion luminescence with a sharp band and long emission lifetimes.[5a,6] In addition, their relative emission intensity can be tuned by control of different combinations of lanthanide dopants and dopant concentration.[6b,c] Consequently, it is reasoned that up-converting rare-earth phosphors (UCPs) constitute one of the most promising classes of luminescent biomaterials with low background fluorescence.

For application in biological labels, UCPs should be small, hydrophilic (or amphiphilic), and easily conjugated with biomolecules. Although up-converting phosphor materials in sizes of several hundreds of nanometers have recently been used in immunohistochemistry in lateral flow (LF) assay

* Corresponding author. Fax: 86-21-55664621. Tel: 86-21-55664185. E-mail: fyli@fudan.edu.cn.

(1) (a) Bruchez, M., Jr.; Moronne, M.; Gin, P.; Weiss, S.; Alivisatos, A. P. *Science* **1998**, *281*, 2013–2016. (b) Chan, W. C. W.; Nie, S. M. *Science* **1998**, *281*, 2016–2018. (c) Van de Rijke, F.; Zijlmans, H.; Li, S.; Vail, T.; Raap, A. K.; Niedbala, R. S.; Tanke, H. J. *Nat. Biotechnol.* **2001**, *19*, 273–276. (d) Michalet, X.; Pinaud, F. F.; Bentolila, L. A.; Tsay, J. M.; Doose, S.; Li, J. J.; Sundaresan, G.; Wu, A. M.; Gambhir, S. S.; Weiss, S. *Science* **2005**, *307*, 538–544. (e) Cai, W. B.; Shin, D. W.; Gheysens, O.; Cao, Q. Z.; Wang, S. X.; Gambhir, S. S.; Chen, X. Y. *Nano. Lett.* **2006**, *6*, 669–676.

(2) (a) Wang, F.; Tan, W. B.; Zhang, Y.; Fan, X. P.; Wang, M. Q. *Nanotechnology* **2006**, *17*, R1−R13. (b) Beaurepaire, E.; Buissette, V.; Sauviat, M. P.; Giaume, D.; Lahlil, K.; Mercuri, A.; Casanova, D.; Huignard, A.; Martin, J. L.; Gacoin, T.; Boilot, J. P.; Alexandrou, A. *Nano. Lett.* **2004**, *4*, 2079–2083.

(3) (a) Denk, W.; Strickler, J.; Webb, W. W. *Science* **1990**, *248*, 73–76. (b) Maiti, S.; Shear, J.; Williams, R. M.; Zipfel, W. R.; Webb, W. W. *Science* **1997**, *275*, 530–532. (c) Heer, S.; Kömpe, K.; Güdel, H. U.; Hasse, M. *Adv. Mater.* **2004**, *16*, 2102–2105. (d) Cai, W. B.; Chen, X. Y. *Small* **2007**, *3*, 1840–1854.

(4) Sertchook, H.; Avnir, D. *Chem. Mater.* **2003**, *15*, 1690–1694.

(5) (a) Auzel, F. *Chem. Rev.* **2004**, *104*, 139–173. (b) Joubert, M. F. *Opt. Mater.* **1999**, *11*, 181–203. (c) Suyver, J. F.; Aebischer, A.; Biner, D. A.; Gerner, P.; Grimm, J.; Heer, S.; Krämer, K. W.; Reinhard, C.; Güdel, H. U. *Opt. Mater.* **2005**, *27*, 1111–1130.

(6) (a) Sivakumar, S.; van Veggel, F. C. J. M.; Raudsepp, M. *J. Am. Chem. Soc.* **2005**, *127*, 12464–12465. (b) Wang, F.; Liu, X. *J. Am. Chem. Soc.* **2008**, *130*, 5642–5643. (c) Ehlert, O.; Thomann, R.; Darbandi, M.; Nann, T. *ACS NANO* **2008**, *2*, 120–124.

10.1021/cm801215t CCC: $40.75
Published on Web 10/29/2008

Scheme 1. Synthetic Route to Amphiphilic mPEG-UCNPs: (a) 3-Chloroperoxybenzoic Acid, Cyclohexane/CH_2Cl_2 (2:1, v/v), Reflux, 3 h; (b) mPEG-OH ($M_t \approx 1900$), RT, 8 h

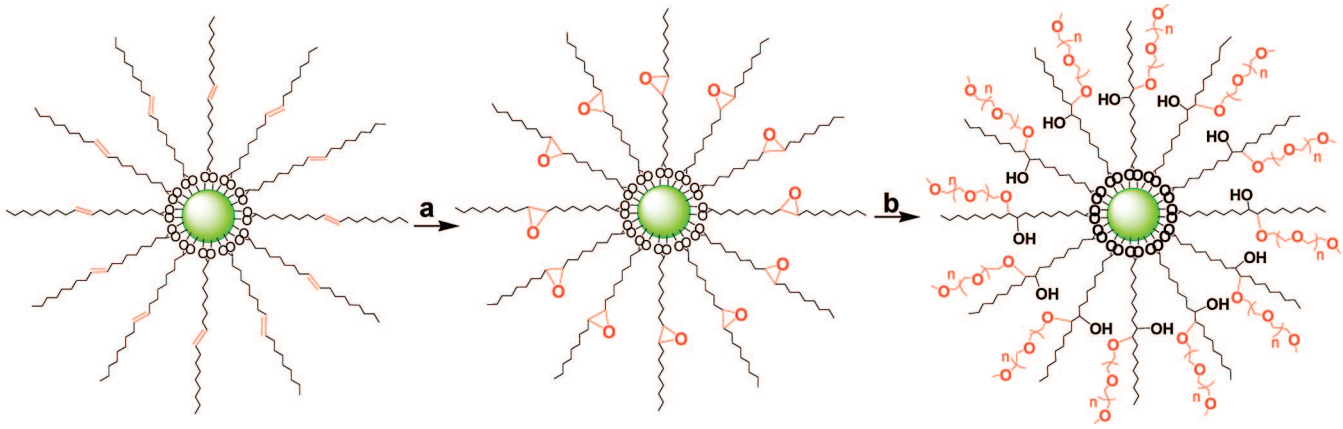

formats and in vitro imaging,[1c,7] these particles are not suitable for the imaging of living cells because of their large size and unsuitable surface characteristics. Also, compared to the great recent advances in the synthetic methods for controlling the nanosize, shape, crystallinity, and monodispersibility of UCNPs bearing hydrophobic surface ligands (such as oleic acid, oleic amine, or linoleic acid),[3c,8] the surface functionalization of UCNPs is mainly limited to the encapsulation of hydrophobic nanoparticles with SiO_2[1d,9] or amphiphilic copolymers.[10] For SiO_2 coatings, precise control over the thickness and shape of the encapsulating SiO_2 layer may be difficult. Alternatively, the hydrophobic UCNPs can be solubilized in water through coating of the nanoparticles with an amphiphilic copolymer.[10] For example, Zhang et al.[10c] reported that coating nanoparticles of size ~50 nm with poly(ethylene imine) allowed their delivery into some cell lines. Chow et al.[10d] also reported that these hydrophobic nanoparticles were rendered hydrophilic by coating them with amphiphilic poly(acrylic acid). In this process, the hydrophobic ends of the amphiphilic copolymer interleave with, rather than replace, the organic groups of the surface layer of the UCNPs, whereas their other ends bear a hydrophilic group.[10a,b,d] However, this hydrophobic interaction is weak, allowing desorption of the polymer molecules from the nanoparticles.[11]

An alternative synthetic strategy for obtaining hydrophilic (or amphiphilic) UCNPs is direct functionalization of the hydrophobic surface ligands by chemical reaction. Very recently, by directly oxidizing oleic acid (OA) ligands with the Lemieux-von Rudloff reagent, a simple and versatile strategy for converting hydrophobic UCNPs into amphiphilic and carboxylic acid-functionalized analogues was developed by our group.[12] However, this method still suffers from some limitations, such as a relatively long reaction time and low yields. Herein, we describe the development of a new and simple strategy for the synthesis of amphiphilic and nonaggregating UCNPs based on epoxidation of their surface OA molecules and further coupling with polyethylene glycol monomethyl ether (mPEG-OH) (Scheme 1). Interestingly, the epoxidation and functionalization processes cause little variation in the morphology and photoluminescence of the UCNPs. Further investigations through cytotoxicity tests and confocal imaging have proved that the amphiphilic mPEG-grafted UCNPs have low cytotoxicity and good cell membrane permeability, which make them promising candidates for use as specific bioimaging agents.

2. Experimental Section

2.1. Materials. Rare earth oxides La_2O_3 (99.999%), Yb_2O_3 (99.999%), and Ho_2O_3 (99.999%) were purchased from Shanghai Yuelong New Materials Co. Ltd. Oleic acid (>90%), polyethylene glycol monomethyl ether (mPEG-OH, $M_t \approx 1900$), and 3-chloroperoxybenzoic acid were purchased from Alfa Aesar Ltd. All other chemical reagents with analytical grade were used directly without further purification. Deionized water was used throughout. Rare earth nitrate stock solutions were prepared by dissolving the corresponding metal oxide in nitric acid at elevated temperature.[8b]

(7) (a) Corstjens, P. L. A. M.; Zuiderwijk, M.; Nilsson, M.; Feindt, H.; Neidbala, R. S.; Tanke, H. J. *Anal. Biochem.* **2003**, *312*, 191–200. (b) Zhang, P.; Rogelj, S.; Nguyen, K.; Wheeler, D. *J. Am. Chem. Soc.* **2006**, *128*, 12410. (c) Lim, S. F.; Riehn, R.; Ryu, W. S.; Khanarian, N.; Tung, C. K.; Tank, D.; Austin, R. H. *Nano. Lett.* **2006**, *6*, 169–174.

(8) (a) Wang, L. Y.; Li, Y. D. *Chem. Mater.* **2007**, *19*, 727–734. (b) Wang, X.; Zhuang, J.; Peng, Q.; Li, Y. D. *Nature* **2005**, *437*, 121–124. (c) Mai, H. X.; Zhang, Y. W.; Si, R.; Yan, Z. G.; Sun, L. D.; You, L. P.; Yan, C. H. *J. Am. Chem. Soc.* **2006**, *128*, 6426–6436. (d) Yi, G. S.; Chow, G. M. *Adv. Funct. Mater.* **2006**, *16*, 2324–2329. (e) Boyer, J. C.; Vetrone, F.; Cuccia, L. A.; Capobianco, J. A. *J. Am. Chem. Soc.* **2006**, *128*, 7444–7445.

(9) (a) Zhang, P.; Rogelj, S.; Nguyen, K.; Wheeler, D. *J. Am. Chem. Soc.* **2006**, *128*, 12410–12411. (b) Zhelev, Z.; Ohba, H.; Bakalova, R. *J. Am. Chem. Soc.* **2006**, *128*, 6324–6325. (c) Rieter, W. J.; Taylor, K.M. L.; Lin, W. *J. Am. Chem. Soc.* **2007**, *129*, 9852–9853. (d) Sivakumar, S.; Van Veggel, F. C. J. M. *Chem. Eur. J.* **2006**, *12*, 5878–5884. (e) Li, Z. Q.; Zhang, Y. *Angew. Chem., Int. Ed.* **2006**, *45*, 7732–7735.

(10) (a) Meiser, F.; Cortez, C.; Caruso, F. *Angew. Chem., Int. Ed.* **2004**, *43*, 5954–5957. (b) Wang, L. Y.; Yan, R. X.; Hao, Z. Y.; Wang, L.; Zeng, J. H.; Bao, J.; Wang, X.; Peng, Q.; Li, Y. D. *Angew. Chem., Int. Ed.* **2005**, *44*, 6054–6057. (c) Chatterjee, D. K.; Rufaihah, A. J.; Zhang, Y. *Biomaterials* **2008**, *29*, 937–943. (d) Yi, G. S.; Chow, G. M. *Chem. Mater.* **2007**, *19*, 341–343.

(11) (a) Aldana, J.; Wang, Y. A.; Peng, X. *J. Am. Chem. Soc.* **2001**, *123*, 8844–8850. (b) Bentzen, E. L.; Tomlinson, I. D.; Mason, J.; Gresch, P.; Warnement, M. R.; Wright, D.; Sanders-Bush, E.; Blakely, R.; Rosenthal, S. J. *Bioconjugate Chem.* **2005**, *16*, 1488–1494. (c) Fan, H.; Leve, E. W.; Scullin, C.; Gabaldon, J.; Tallant, D.; Bunge, S.; Boyle, T.; Wilson, M. C.; Brinker, C. J. *Nano Lett.* **2005**, *5*, 645–648. (d) Dubertret, B.; Skourides, P.; Norris, D. J.; Noireaux, V.; Brivanlou, A. H.; Libchaber, A. *Science* **2002**, *298*, 1759–1762.

(12) Chen, Z. G.; Chen, H. L.; Hu, H.; Yu, M. X.; Li, F. Y.; Zhang, Q.; Zhou, Z. G.; Yi, T.; Huang, C. H. *J. Am. Chem. Soc.* **2008**, *130*, 3023–3029.

2.2. Synthesis of Up-Converting Rare-Earth Nanophosphors (UCNPs). *2.2.1. Synthesis of Hydrophobic Oleic-Acid-Capped UCNPs.* All of the doping ratios of Ln^{3+} in our experiments were molar. In a typical procedure, sodium oleate (30 mmol), deionized water (6 mL), ethanol (12 mL), and oleic acid (26 mmol) were mixed together under agitation to form a homogeneous solution. An aqueous solution of rare-earth nitrate ($Ln(NO_3)_3$, Ln: 85% mol La, 12% mol Yb, 3% mol Er or 79% mol La, 20% mol Yb, 1% mol Ho) (1 mmol; total amount) was then added under magnetic stirring. Subsequently, aqueous NH_4F solution (5 mL) was added dropwise. The resulting mixture was agitated for about 10 min and then transferred to a 50 mL autoclave, which was sealed and maintained at 170 °C for 10 h. The system was allowed to cool to room temperature naturally, whereupon the products were deposited at the bottom of the vessel. Cyclohexane was used to dissolve and collect the products. By adding ethanol to the sample-containing cyclohexane solution, the products were reprecipitated. The precipitates were separated by centrifugation. Pure powders could be obtained by purifying the precipitates by washing with ethanol several times to remove oleic acid, sodium oleate, and other residual compounds.

2.2.2. Converting Hydrophobic Oleic-Acid-Capped UCNPs into Hydrophilic Ones. The as-prepared LaF_3:20% Yb, 1% Ho or LaF_3:12% Yb, 3% Er nanoparticles (100 mg) were dispersed in 30 mL of a mixture of cyclohexane and CH_2Cl_2 (2:1, v/v), and then 3-chloroperoxybenzoic acid (25 mg) was added as a peroxide reagent. After refluxing for 3 h, the reaction mixture was cooled to room temperature, whereupon polyethylene glycol monomethyl ether (mPEG-OH, $M_t \approx 1900$, 1.3 g) was added and the resulting mixture was stirred for 8 h at room temperature. The solvents were then removed under reduced pressure, and the product was washed alternately with deionized water and ethanol, three times with each, and stored either in deionized water or ethanol.

2.3. Cell Culture. A human nasopharyngeal epidermal carcinoma cell line (KB cell) was provided by the Institute of Biochemistry and Cell Biology, SIBS, CAS (China). Cells were grown in RPMI 1640 (Roswell Park Memorial Institute's medium) supplemented with 10% FBS (fetal bovine serum) at 37 °C and 5% CO2. Cells (5×10^8/L) were plated on 14 mm glass coverslips under 100% humidity and allowed to adhere for 24 h.

2.3.1. Cytotoxicity of mPEG-UCNPs. In vitro cytotoxicity was measured by performing methyl thiazolyl tetrazolium (MTT) assays on the KB cells. Cells were seeded into a 96-well cell culture plate at 5 × 104/well, under 100% humidity, and were cultured at 37 °C and 5% CO_2 for 24 h; different concentrations of UCNPs (0, 125, 250, and 500 μg/mL, diluted in RPMI 1640) were then added to the wells. The cells were subsequently incubated for 4 or 24 h at 37 °C under 5% CO_2. Thereafter, MTT (10 μL; 5 mg/mL) was added to each well and the plate was incubated for an additional 4 h at 37 °C under 5% CO_2. After the addition of 10% sodium dodecyl sulfate (SDS, 100 μL/well), the assay plate was allowed to stand at room temperature for 12 h. The OD570 value (Abs.) of each well, with background subtraction at 690 nm, was measured by means of a Tecan Infinite M200 monochromator-based multifunction microplate reader. The following formula was used to calculate the inhibition of cell growth: Cell viability (%) = (mean of Abs. value of treatment group/mean Abs. value of control) × 100%.

2.3.2. Cellular Staining. To ensure complete dispersion of the mPEG-UCNPs in the serum-free media, their solutions (100 or 500 μg/mL) obtained from a stock suspension were sonicated for 30 min.

For single-label imaging, KB cells were stained with 100 μg/mL PEG-UCNPs in a 5% CO_2 incubator at 4 or 37 °C for 2 h. Living cell imaging was then carried out after washing the cells with PBS once more to remove the excess mPEG-UCNPs.

For multilabel imaging, KB cells were first stained with 5 μM 1,1′-dioctadecyl-3,3,3′,3′-tetramethylindocarbocyanine perchlorate (DiI, $\lambda_{max}^{em} = 575$ nm, FMHW = 35 nm, see Figure S1 in the Supporting Information) in Ca/Mg-free PBS buffer for 20 min at 37 °C under 5% CO_2. After washing the cells with PBS, the chamber slide was incubated with 500 μg/mL PEG-UCNPs in a 5% CO_2 incubator at 37 °C for 2 h. Finally, after washing the cells with PBS once more to remove the excess mPEG-UCNPs, the cells were fixed and their nuclei were stained with 4′,6-diamidine-2′-phenylindole dihydrochloride (DAPI) ($\lambda_{max}^{em} = 465$ nm, see Figure S1 in the Supporting Information; DAPI is an organic fluorophore that shows a blue fluorescence when bound to DNA).

2.3.3. Confocal Imaging of mPEG-UCNPs-Incubated Living Cells. Confocal imaging of cells was performed with a modified Olympus FV1000 laser scanning confocal microscope (LSCM) equipped a continuous-wave (CW) NIR laser operating at 980 nm (Connet Fiber Optics, China). A 60× oil-immersion objective lens was used. Excitation of DAPI was carried out with a semiconductor laser at 405 nm, and its emission was collected at 460 ± 20 nm. DiI was excited at 543 nm using an HeNe laser, and its emission was collected at 580 ± 20 nm. For the UCNPs, the CW NIR laser operating at 980 nm provided the excitation, and emission was collected at 520 ± 80 nm.

2.4. Characterization. Powder X-ray diffraction (XRD) measurements were performed on a Bruker D4 diffractometer at a scanning rate of 1°/min in the 2θ range from 10 to 70° (Cu Kα radiation, $\lambda = 1.54056$ Å). The size and morphology of UCNPs were determined at 200 kV at a JEOL JEM-2010 low to high resolution transmission electron microscope (HR-TEM). These as prepared samples were dispersed in cyclohexane and dropped on the surface of a copper grid for TEM test. Energy-dispersive X-ray analysis (EDXA) of the samples was also performed during HRTEM measurements. ^{1}H NMR spectra were recorded on a Varian Mercury 400 spectrometer. Proton chemical shifts are reported in parts per million downfield from tetramethylsilane (TMS). FTIR spectra were performed using an IRPRESTIGE-21 spectroscope (Shimadzu) with KBr pellets. Thermogravimetric analysis (TGA) curves were recorded on a DTG-60H (Shimadzu) at a heating rate of 10 °C/min. The upconversion luminescence emission spectra were recorded on Edinburgh LFS-920 instrument, but the excitation source using an external 0−1 W adjustable 980 nm semiconductor laser (Beijing Hi-Tech Optoelectronic Co., China) with an optic fiber accessory, instead of the Xeon source in the spectrophotometer. The upconversion luminescence images were acquired digitally on a Nikon multiple CCD camera. Dynamic light scattering (DLS) experiments were carried out on an ALV-5000 spectrometer-goniometer equipped with an ALV/LSE-5004 light scattering electronic and multiple tau digital correlator and a JDS Uniphase He−Ne laser (632.8 nm) with an output power of 22 mW. The size distribution was measured at 25 °C with a detection angle of 90°.

3. Results and Discussion

3.1. Synthesis and Characterization of UCNPs. Because of the high ionicity of the La^{3+} to fluoride bond, LaF_3 has very low vibrational energies and has been used as a promising up-conversion luminescence host matrix over the past decade.[13] In the present work, OA-capped LaF_3:20%

(13) Lezhnina, M. M.; Jüstel, T.; Kätker, H.; Wiechert, D. U.; Kynast, U. H. *Adv. Funct. Mater.* **2006**, *16*, 935–942.

Yb, 1% Ho and LaF_3:12% Yb, 3% Er were synthesized by a modified hydrothermal route.[14] All of the OA capped up-converting nanophosphors could be well-dispersed in a nonpolar solvent (such as cyclohexane, chloroform, or dichloromethane) and then deposited by the addition of a polar solvent (ethanol or acetone). The surfaces of the nanoparticles were coated with ~10 wt% OA, as characterized by thermogravimetric analysis (TGA) (Figure S2 in the Supporting Information).

Epoxidation of a carbon−carbon double bond, as a classical organic reaction, has been widely used in chemical processes.[15] The carbon−carbon double bond can be easily epoxidized with peroxide reagents to give a three-membered-ring epoxide, and the highly reactive epoxide product may then be rapidly reacted with many reactive groups, such as −OH,[16] −SH,[17] $-NH_2$,[18] or −COOH.[15b,19] Meanwhile, nanoparticles with PEG-functionalized exteriors generally exhibit much lower toxicity, are nonimmunogenic and nonantigenic, and display longer circulation times.[11b,c] On the basis of the above facts, in the present work, the hydrophobic OA-capped up-converting nanophosphors were converted to amphiphilic analogues by first using 3-chloroperoxybenzoic acid as a peroxide reagent to epoxidize the surface ligands (oleic acid) to three-membered-ring epoxide compounds, and these were then further coupled with polyethylene glycol monomethyl ether (mPEG-OH, Mt ≈ 1900) (Scheme 1). Herein, as one example of up-converting nanophosphors (UCNPs), LaF_3: 20% Yb, 1% Ho nanoparticles were investigated in detail, and the oleic-acid-capped, epoxidized octadecyl-alkyl-capped, and mPEG-capped UCNPs are denoted as OA-UCNPs, EOA-UCNPs, and mPEG-UCNPs, respectively.

Successful epoxidation of the carbon−carbon double bond of the surface OA ligand was verified by ^{1}H NMR and Fourier transform infrared (FTIR) analyses. To avoid the interference of the dopant ions (Yb^{3+}, Ho^{3+}, and Er^{3+}) on the ^{1}H NMR signal, herein, the pure LaF_3 nanoparticles were chosen to replace UCNPs for the ^{1}H NMR study. Figure 1 shows the evolution of the ^{1}H NMR spectra of the changing ligands on the surface of the pure LaF_3 nanoparticles. All samples were dispersed in $CDCl_3$ to enable direct comparison of the spectra. Well-known in the field of colloidal nanoparticles, the NMR peaks of surface ligands are significantly broader than those of the corresponding free ligands.[20] As shown in Figure 1A, the characteristic resonance with a chemical shift of $\delta = 5.32$ ppm, corresponding to the carbon−carbon double bond in OA, is clearly observed in

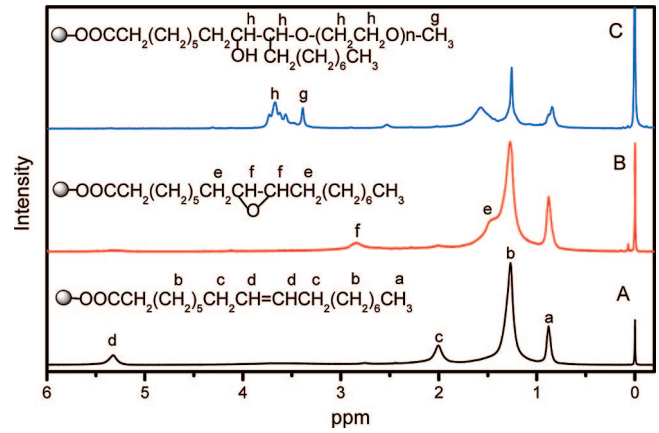

Figure 1. ^{1}H NMR spectra ($CDCl_3$ solutions) of (A) LaF_3 nanoparticles capped with hydrophobic oleic acid groups, (B) ligands with epoxidized double bonds, and (C) amphiphilic mPEG grafted ligands.

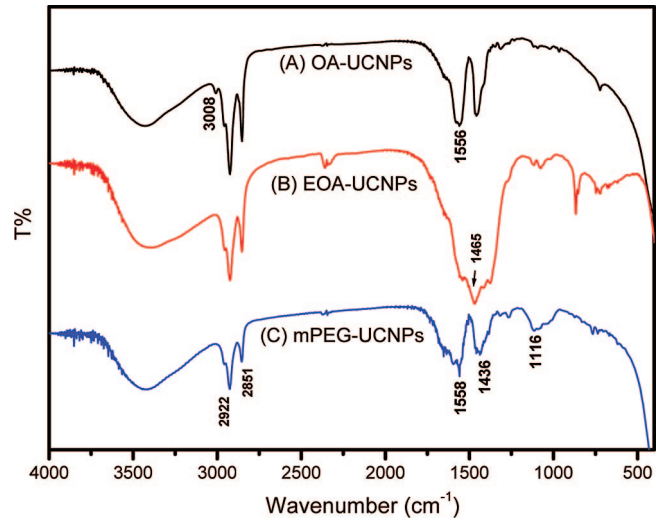

Figure 2. FTIR spectra of the nanoparticles: (A) OA-UCNPs, (B) EOA-UCNPs, and (C) mPEG-UCNPs.

the ^{1}H NMR spectrum of the pure OA-capped LaF_3nanoparticles. After treatment with 3-chloroperoxybenzoic acid, the resonance at 5.32 ppm disappeared (Figure 1B) and two new peaks centered at 2.84 and 1.47 ppm appeared, indicating formation of the epoxide. Following further reaction with mPEG-OH, a broad peak appeared in the range from $\delta = 3.38$ to 3.73 ppm, attributable to -OCH_3 and $-(OCH_2CH_2)_n-$ of the mPEG backbone, which was accompanied by the disappearance of the epoxide peaks at 2.84 and 1.47 ppm, as shown in Figure 1C, suggesting the successful grafting of mPEG through epoxide ring-opening.

The epoxidation process of the surface OA ligand of the UCNPs was also investigated by Fourier-transform infrared (FTIR) spectroscopy. Figure 2 shows the FTIR spectra of the three UCNP samples, i.e., OA-UCNPs, EOA-UCNPs, and mPEG-UCNPs. These three UCNP samples exhibit a broadband at around $\nu = 3450$ cm^{-1}, corresponding to the O−H stretching vibration. The transmission bands peaked

(14) (a) Wang, X.; Zhuang, J.; Peng, Q.; Li, Y. D. *Inorg. Chem.* **2006**, *45*, 6661–6665. (b) Yi, G. S.; Chow, G. M. *J. Mater. Chem.* **2005**, *15*, 4460–4464.
(15) (a) Findley, T. W.; Swern, D.; Scanlan, J. T. *J. Am. Chem. Soc.* **1945**, *67*, 412–414. (b) Mack, C. H.; Bickford, W. G. *J. Org. Chem.* **1953**, *18*, 686–692. (c) Gelb, L.; Port, W.; Ault, W. *J. Org. Chem.* **1958**, *23*, 2022–2023.
(16) Fujioka, H.; Hirose, H.; Ohba, Y.; Murai, K.; Nakahara, K.; Kita, Y. *Tetrahedron* **2007**, *63*, 625–637.
(17) Niel, G.; Escale, R.; Vidal, J. P.; Rechencq, E.; Girard, J. P.; Rossi, J. C. *Tetrahedron Lett.* **1991**, *32*, 2613–2614.
(18) Yadav, J. S.; Bandyopadhyay, A.; Reddy, B. V. S. *Tetrahedron Lett.* **2001**, *42*, 6385–6388.
(19) Burgos, C. E.; Ayer, D. E.; Johnson, R. A. *J. Org. Chem.* **1987**, *52*, 4973–4977.
(20) (a) Ji, X. H.; Copenhaver, D.; Sichmeller, C.; Peng, X. G. *J. Am. Chem. Soc.* **2008**, *130*, 5726–5735. (b) Sachleben, J. R.; Wooten, E. W.; Emsley, L.; Pines, A.; Colvin, V. L.; Alivisatos, A. P. *Chem. Phys. Lett.* **1992**, *198*, 431–436. (c) Holland, G. P.; Sharma, R.; Agola, J. O.; Amin, S.; Solomon, V. C.; Singh, P.; Buttry, D. A.; Yarger, J. L. *Chem. Mater.* **2007**, *19*, 2519–2526.

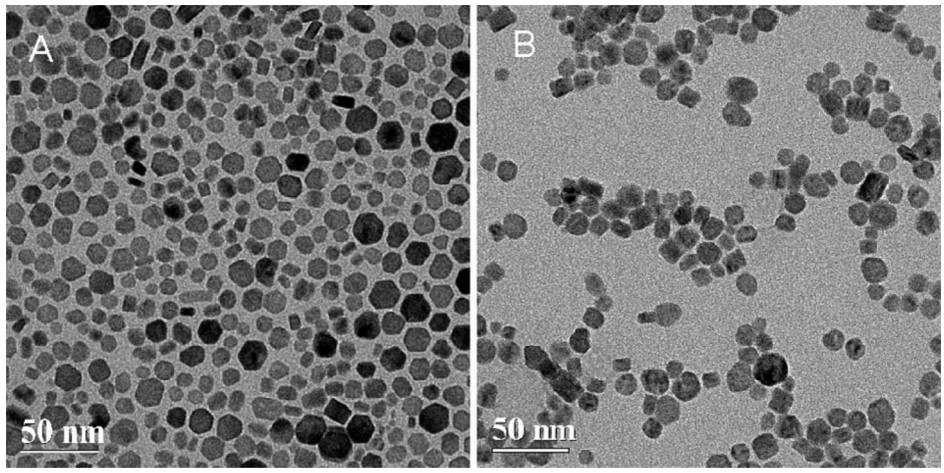

Figure 3. TEM images of (A) OA-UCNPs and (B) mPEG-UCNPs from dispersions in cyclohexane and ethanol, respectively.

at approximately 2922 and 2851 cm^{-1} for each of the samples may be assigned to the asymmetric (ν_{as}) and symmetric (ν_s) stretching vibrations, respectively, of methylene (CH_2) in the long alkyl chain.[12] As shown in Figure 2A, a peak at ν = 3008 cm^{-1}, attributable to =C−H stretching vibration, can clearly be seen in the spectrum of the OA-UCNPs sample;[12] however, this feature is apparently lost in the spectrum of the oxidized EOA-UCNPs sample (Figure 2B), suggesting the disappearance of the −HC=CH− group. At the same time, broad asymmetric (υ_{as}) stretching vibrational bands in the range of 1548−1370 cm^{-1} are observed in the spectrum of EOA-UCNPs (Figure 2B). These observations were also indicative of the formation of the three-membered epoxide ring. After further reaction with mPEG-OH, the characteristic bands of the three-membered epoxide ring disappeared and new peaks appeared at ν = 1558, 1436, and 1116 cm^{-1}, thus corroborating successful synthesis of the amphiphilic mPEG-UCNPs by this strategy.

Furthermore, the dependence of the epoxidation process on the morphology and size of the UCNPs was investigated in detail. Figure 3 shows transmission electron microscopy (TEM) images of the OA-UCNPs and mPEG-UCNPs (LaF_3: 20% Yb, 1% Ho). The monodisperse nanoparticles of the OA-UCNPs with sizes of ∼15 nm suggest that the long-chain oleic acid ligands on the crystal surface play a critical role[8c] in preventing aggregation (Figure 3A). After epoxidation and further reaction with mPEG-OH, the UCNP samples could be well dispersed in both polar solvents (such as ethanol or water) and solvents of low polarity (such as $CHCl_3$), indicating the amphiphilic nature of the mPEG-OH-grafted UCNPs. As shown in Figure 3B, the formation of nanoarrays was no longer seen owing to introduction of the hydrophilic PEG groups on the surface ligands, but the mPEG-OH-grafted UCNP samples, i.e., mPEG-UCNPs, were still seen to consist primarily of single nanoparticles of diameter of ∼15 nm. Moreover, compared with our previously reported azelaic acid-capped UCNP samples,[12] mPEG-UCNPs showed better monodispersity, indicating their amphiphilic nature, because of the coexistence of the long alkyl groups and mPEG-OH functions. The interactions of the long octadecyl chains prevent the formation of aggregates.

In a further investigation, the hydrodynamic diameter of OA-UCNPs was compared with that of mPEG-UCNPs by dynamic light scattering (DLS). As shown in Figure 4, the effective hydrodynamic diameter of mPEG-UCNPs was measured as 25.6 nm, whereas that of OA-UCNPs was measured as 17 ± 3 nm. Generally, when they are bound to the surface of nanoparticles, PEG polymers tend to be extended by 20−30% compared to their native structures;[21] the hydrodynamic diameter of the mPEG-UCNPs was estimated to be 26.8 nm. The increase in hydrodynamic diameter was consistent with estimated data for mPEG-OH UCNPs samples, indicating successful grafting of the mPEG-OH onto the oleic acid.

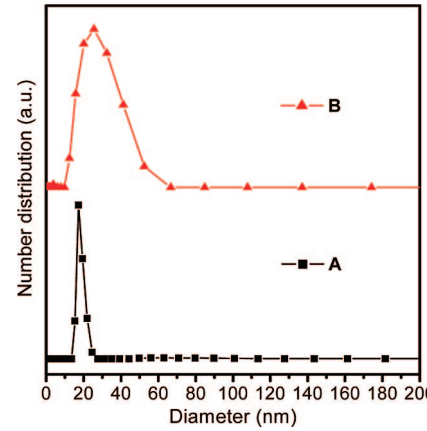

Figure 4. Diameter distribution of (A) OA-UCNPs and (B) mPEG-UCNPs, determined by dynamic light scattering.

Energy-dispersive X-ray analysis (EDXA) patterns and XRD patterns of both OA-UCNPs and mPEG-UCNPs were also studied to investigate the effects of the epoxidation process. The EDXA patterns (Figure S3) confirmed the presence of La, Yb, and F in both samples, and the large amounts of C and O evident from the spectra indicated the presence of the organic ligands coated on the surface of the UCNPs. XRD patterns (Figure S4) also demonstrated that the samples were of pure hexagonal phase LaF_3 (JCPDS card 72−1435) with good crystallinity, which is very beneficial for obtaining bright luminescence. Therefore, it can be concluded that the epoxidation has no obvious adverse effects on the composition of the UCNPs.

(21) Mori, S.; Barth, H. G. *Size Exclusion Chromatogrphy*, 1st ed.; Springer: Berlin, 1999.

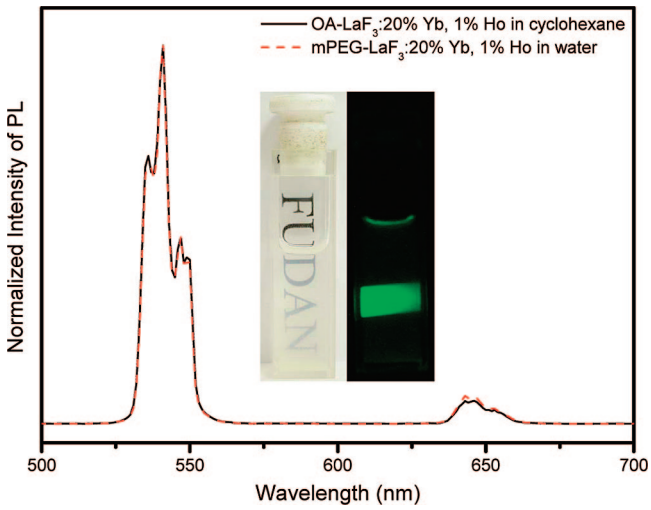

Figure 5. Room-temperature up-conversion luminescence spectra of OA-UCNPs (2 mg/mL) in cyclohexane and mPEG-UCNPs in water under CW excitation at 980 nm (power ≈ 800 mW). Inset: a visual photograph of mPEG-UCNP shows an almost pure green color.

As a result of the surface functionalization of the mPEG-UCNPs, all samples could be well dispersed in some polar organic solvents such as water, DMF, or DMSO (Figure 5 and the Supporting Information, Figure S5) as well as in solvents of low polarity (such as $CHCl_3$), due to the coexistence of the long alkyl groups and PEG moieties. Herein, we pay more attention to the luminescent properties of the mPEG-UCNPs in aqueous solution. Under CW excitation at 980 nm (power ≈ 800 mW), the room temperature up-conversion luminescence spectra of the mPEG-UCNPs (LaF_3: 20% Yb, 1% Ho) in water (2 mg/mL) were measured. Bright-green emissions at 541 nm, corresponding to the $^5S_2 \rightarrow {}^5I_8$ transition, and very weak red emissions at 643 nm, attributable to the $^5F_5 \rightarrow {}^5I_8$ transition, were observed in both cyclohexane and water.[22] The up-conversion luminescence properties of LaF_3: 20% Yb, 1% Ho showed no obvious changes before and after surface modification. Similar effects were also found for mPEG-LaF_3:12% Yb, 3% Er samples (Figures S8 and S9 in the Supporting Information). These results indicated that the UCNPs were stable throughout the process of epoxidation and further functionalization. The inset in Figure 5 shows up-conversion luminescence photographs of a 2 wt % colloidal solution of LaF_3: 20% Yb, 1% Ho in water under CW excitation at 980 nm (power density ≈ 0.3 W/mm^2), which are nearly pure green in color. In addition, the amphiphilic mPEG-UCNPs were found to be very stable in water and physiological buffers. Also, no obvious luminescence density change was observed over a wide pH range (pH 3−9, Figures S10 and S11in the Supporting Information), indicating excellent stability and pH-independent luminescence properties of the UCNPs as compared to organic dyes and semiconductor QDs. The good stability of these UCNPs may be attributed to their amphiphilic surface ligands. The mPEG was grafted onto the oleic acid in an interleaving arrangement; this structure may limit the interactions between the hydrophobic tails and the surfaces of the nanoparticles.

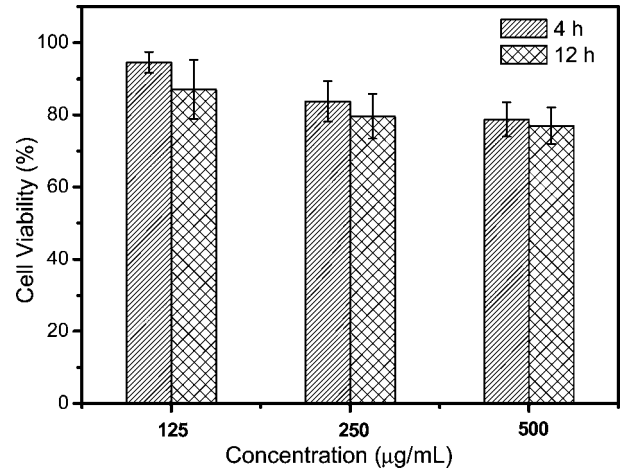

Figure 6. In vitro cell viability of KB cells incubated with mPEG-UCNPs at different concentrations for 4−12 h.

3.2. Applications as Luminescent Biological Labels. Generally, the cytotoxicity and cell-permeability characteristics of fluorescent materials are critical to the application of such materials as bioprobes. In the present work, the effect of the mPEG-UCNPs (LaF_3: 20% Yb, 1% Ho) on cell proliferation was assessed with KB cells using an in vitro toxicology assay kit (TOX-1, Sigma) based on the reduction activity of methyl thiazolyl tetrazolium (MTT) (Figure 6). The viability of untreated cells was assumed to be 100%. Upon incubating the KB cells with 125 μg mL^{-1} mPEG-UCNPs, less than 15% of the cells died after a 12 h exposure. When the concentration of mPEG-UCNPs was increased to 250 μg mL^{-1}, the cell viability still remained above 80%. These data show that the mPEG-UCNPs ($\leq$250 μg mL^{-1}) can be considered to have low cytotoxicity, which is in agreement with a previous report that the rare-earth elements have good chemical stability and generally low toxicity.[23]

By utilizing a modified laser scanning confocal microscope (LSCM) equipped with CW excitation at 980 nm, the further practical application of mPEG-UCNPs in the luminescence imaging of living cells was investigated. The KB cells showed negligible background fluorescence (data not shown). However, after incubation with 100 μg/mL mPEG-UCNPs in PBS (pH 7) for 10 min at 25 °C, intense intracellular luminescence was observed (Figure 7A). Spectrum scan experiments showed that the maximum emission wavelengths of the luminescence after incubation with mPEG-UCNPs were at 541 and 643 nm (Figure S12 in the Supporting Information), thus confirming that the intracellular luminescence could be attributed to the mPEG-UCNPs. Additionally, brightfield measurements after the treatment with mPEG-UCNPs confirmed that the cells were viable throughout the imaging experiments (Figure 7B). Overlays of confocal luminescence and brightfield images further demonstrated that the luminescence was evident in the intracellular region (Figures 7C), suggesting that the mPEG-UCNPs were internalized into the cells rather than merely staining the

(22) (a) Lahoz, F.; Martin, I. R.; Alonso, D. *Phys. Rev. B* **2005**, *71*, 051106. (b) Lahoz, F.; Martin, I. R.; Briones, A. *J. Appl. Phys.* **2004**, *95*, 2957.

(23) (a) Palmer, R. J.; Butenhoff, J. L.; Stevens, J. B. *Environ. Res.* **1987**, *43*, 142. (b) Larson, D. R.; Zipfel, W. R.; Williams, R. M.; Clark, S. W.; Bruchez, M. P.; Wise, F. W.; Webb, W. W. *Science* **2003**, *300*, 1434–1436.

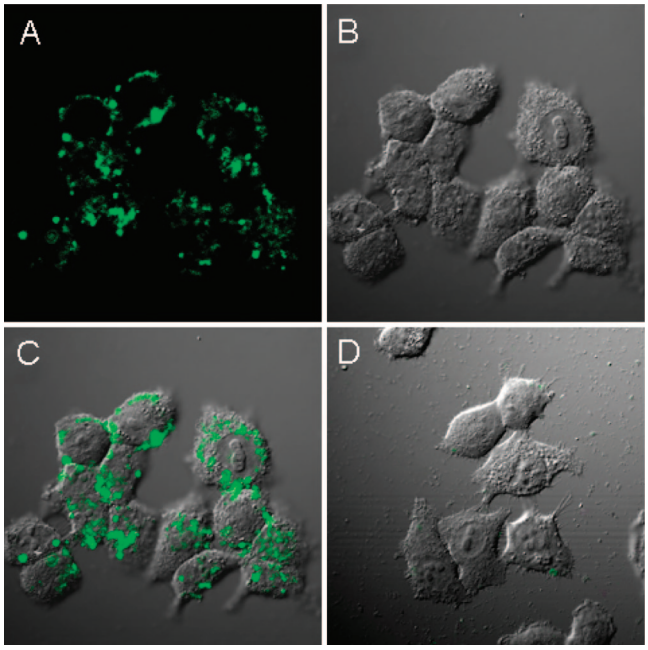

Figure 7. Confocal luminescence and bright-field images of KB cells. (A) Confocal luminescence images of cells stained with 100 μg mL^{-1} mPEG-UCNPs for 2 h at 37 °C (λ_{ex} = 980 nm). (B) Bright-field image of cells shown in panel a. (C) Overlay image of (A) and (B). (D) Overlay image of confocal luminescence and brightfield images of cells stained with 100 μg mL^{-1} mPEG-UCNPs (green) for 2 h at 4 °C.

membrane surface. This was further confirmed by the fact that very weak intracellular up-conversion luminescence was measured in a control experiment at 4 °C (Figure 7D).

Generally, because of its high density, rare-earth fluoride nanoparticle was easily sunk down in solution. So, it is reasoned that upconverting nanophosphors based on rare-earth fluoride easily become sedimentation on the member surface and outside of the cells. For example, in the bioimaging for PEI-coating $NaYF_4$: Yb, Er nanoparticles (with size of $\sim$ 50 nm),[10c] some non-intercellular signals were obviously observed, indicating that some PEI-coating $NaYF_4$: Yb, Er nanoparticles becomes sedimentation outside of the cells. In our case, however, no upconversion luminescence signal outside of the KB cells was measured the cell imaging although the density of hexagonal $P_{6322}(182)$ phase LaF_3 is 5.992 g/cm^3, which would attributed to the amphiphilic coating layer on the surface of UCNPs.

To further confirm that the origin of the observed luminescence signal (green) was located intracellularly (on the same axis as the nuclear stain) rather than in material adsorbed onto the cell surface, confocal luminescence imaging was carried out on multilabeled KB cells costained with the blue fluorescent dye DAPI, the red fluorescent dye DiI, and mPEG-UCNPs (for details, see the Experimental Section). The cell cytoplasm was stained red with DiI, and the nuclei were stained blue with DAPI. The LSCM optical setup was operated in multichannel mode (see Figure S13 in the Supporting Information). By sequential selective excitation at 405, 543, and 980 nm, we could obtain confocal imaging by collection at 460 $\pm$ 20 (for DAPI), 580 $\pm$ 20 (for DiI), and 520 $\pm$ 80 nm (for UCNPs), respectively, as shown in Figure S14 in the Supporting Information. Furthermore, confocal imaging data collected as a series along the *Z*-optical axis (*Z*-stack) indicated that the intracellular and perinuclear localization of the mPE-UCNPs (green) signal was in the same focal plane as the nuclear stain (Figure S15 in the Supporting Information), which verified that the up-converting luminescence signal of the mPEG-UCNPs was indeed localized within the cell. In this way, mPEG-UCNPs may be used as cell-permeable dyes for luminescent staining in living cells. The facile internalization of the mPEG-OH-capped UCNPs by cells may be related to the lipophilicity (long alkyl group) and water-solubility (mPEG-OH) of these labels.

In addition, as is evident from Figure S14A of the Supporting Information, although the broad luminescence collection channel (520 $\pm$ 80 nm) of the UCNPs overlaps with the collection channels of DiI and DAPI, no fluorescence signals from DiI and DAPI were measured under the CW excitation at 980 nm, indicating that the UCNPs provide an extremely high sensitivity of imaging. Such observations make amphiphilic UCNPs extremely promising candidates for use in bioimaging.

4. Conclusions

In summary, a simple, effective, and versatile method has been developed for converting hydrophobic UCNPs into amphiphilic ones. The as-prepared amphiphilic UCNPs have proved to be very stable and retain the same properties as those that are soluble in organic solvents. Moreover, the incorporation of the mPEG groups improves the biocompatibility of the UCNPs, and the mPEG-UCNPs can readily permeate through cell membranes. LSCM images have shown no background noise within cells, making the amphiphilic mPEG-UCNPs promising candidates for use as specific bioimaging agents. It should be possible to extend this method to other nanomaterials that are coated with surfactants that incorporate carbon−carbon double bonds, such as oleic acid or linoleic acid. Moreover, the highly reactive three-membered-ring epoxide intermediates may also be further functionalized with other groups, such as −SH, $-NH_2$, or −COOH, allowing their incorporation into the surface coating by chemical bonding.

Acknowledgment. The authors thank NSFC (20490210 and 20775017), NHTPC (2006AA03Z318), NCET-06-0353, Shanghai Leading Academic Discipline Project (B108), Shanghai Science and Technology Community (06QH14002), and Huo Yingdong Education Foundation (104012) for financial support. We also thank Dr. Xianzhong Zhang and Xinfang Duan of Beijing Normal University for helpful discussion.

Supporting Information Available: TGA curves, EDXA spectra, XRD patterns, Size distribution, TEM characterization, luminescence spectra and photographs of UCNPs; photographs of colloidal solutions of UCNPs in $CHCl_3$, DMF and DMSO; luminescence spectra of UCNPs in phosphate buffered saline (PBS) solutions with different pH values; luminescent spectrum of UCNPs during confocal imaging; multilabeled KB cells and *Z*-stack confocal imaging; schematic layout of the light path in the modified laser scanning confocal microscope (LSCM) (PDF). This material is available free of charge via the Internet at http://pubs.acs.org.

CM801215T